Arch Appl Mech (2016) 86:1715–1732
DOI 10.1007/s00419-014-0972-5

CrossMark

SPECIAL

Oliver Heuss · Rogério Salloum · Dirk Mayer · Tobias Melz

Tuning of a vibration absorber with shunted piezoelectric transducers

Received: 16 December 2013 / Accepted: 19 November 2014 / Published online: 13 December 2014
© The Author(s) 2014. This article is published with open access at Springerlink.com

Abstract In order to reduce structural vibrations in narrow frequency bands, tuned mass absorbers can be an appropriate measure. A quite similar approach which makes use of applied piezoelectric elements, instead of additional oscillating masses, are the well-known resonant shunts, consisting of resistances, inductances, and possibly negative capacitances connected to the piezoelectric element. This paper presents a combined approach, which is based on a conventional tuned mass absorber, but whose characteristics can be strongly influenced by applying shunted piezoceramics. Simulations and experimental analyses are shown to be very effective in predicting the behavior of such electromechanical systems. The vibration level of the absorber can be strongly attenuated by applying different combinations of resistant, resonant, and negative capacitance shunt circuits. The damping characteristics of the absorber can be changed by applying a purely resistive or resonant resistant shunt. Additionally, the tuning frequency of the absorber can be adapted to the excitation frequency, using a negative capacitance shunt circuit, which requires only the energy to supply the electric components.

Keywords Shunt damping · Tuned mass absorber · Active vibration control · Semi-active · Frequency tuning

1 Introduction

Tuned vibration absorbers [1] are common means of vibration reduction in many technical applications. Basically, those devices are single degree of freedom oscillators comprising of a spring-damper element and of an inertial mass. Usually, the vibration absorber is tuned to a resonance frequency of the vibrating structure that it is attached to, or to a dominating excitation frequency. Tuning rules for the resonance frequency and the damping have been derived [2]. It is also well known that the ratio of the absorber's mass to the effectively vibrating mass of the host structure influences the bandwidth of the achievable vibration reduction. In case of a varying disturbance frequency or uncertainties in the resonance of the host structure, a large oscillating mass would be required to ensure a certain performance. Since a large additional mass is not acceptable in many applications, adaptive tuned vibration absorbers have been developed. Generally, the resonance of the oscillator can be adjusted by varying the mass or the stiffness. An overview of several designs can be found in [3]. Mostly,

O. Heuss (✉) · R. Salloum · D. Mayer · T. Melz
Smart Structures, Fraunhofer Institute for Structural Durability and System Reliability LBF, Bartningstraße 47,
64289 Darmstadt, Germany
E-mail: oliver.heuss@lbf.fraunhofer.de

R. Salloum
E-mail: rogerio.salloum@lbf.fraunhofer.de

D. Mayer
E-mail: dirk.mayer@lbf.fraunhofer.de

mechatronic actuators, like servo motors, are used to adjust the geometry of the spring element and in turn the resonance. Such designs have the advantage of using well-established actuators. Furthermore, the device can be treated as being fully passive after being tuned to the target frequency. However, the speed of adaptation is limited by the motor. Since the tuned vibration absorber is applied to a location where high vibration levels occur, issues of reliability are also raised by this design. Alternatively, the integration of dynamic actuators has been proposed, e.g., piezoelectric patches or multilayer actuators. Since nearly no movable parts are necessary, the design is much simpler and can withstand a high number of fatigue cycles [4]. Adaptation of the absorber parameters is realized by variation of the gain of a feedback loop, resulting in high adaptation speeds [5]. A clear drawback of those systems is the permanent need for electrical power to drive the actuators when using the absorber for frequencies away from the passive state.

In the last decades, much research has been done to understand and design the so-called "shunted systems". By applying electrical shunt circuits to piezoelectric transducers, their mechanical properties can be changed without the need of actively driven piezoelectric actuators. One of the most basic concepts introduced by [6], the resistive resonant shunt, behaves similar as a tuned mass absorber. That way, a very flexible absorption device can be set up, with the possibility of tuning it only by changing the properties of some electric components. Nevertheless, these techniques are yet not integrated in many technical structures. One reason for this might be the high design effort. There are many design parameters, each affecting each other, which have to be optimized in order to get a technical applicable solution. Additionally, the performance is usually limited by geometric boundaries for the application of the piezoelectric elements, as well as the material properties of present piezoelectric elements.

This article describes the design process of a system, which is a combination of a classical tuned mass absorber and an electrically shunted piezoelectric transducer. The basic absorption effect is achieved with the tuned mass absorber, and the characteristics are changed by the type and configuration of the shunts connected to the transducers. One of the semi-passive techniques, which are applied for that purpose, is the above-mentioned resistive resonant shunt (RL-shunt). Additionally, the stiffness of the piezoelectric transducer is varied using capacitive shunts. This effect has already been exploited based on passive elements to alter the resonance of a piezoelectric vibration absorber [7]. In this paper, different semi-passive and semi-active shunting techniques are applied and used in three different ways, to change the fundamental behavior of the tuned mass absorber: First, a simple resistant (R-shunt) and an RL-shunt are connected to piezoelectric elements, which are bonded to the absorber structure, to change the damping behavior of the absorber. Second, a resonant shunt, in combination with a negative capacitance, which is thoroughly described in [8] and [9], is used to attenuate the absorber's vibration, thus making it possible to achieve a structural behavior, which is nearly equivalent to that of a stiffly coupled additional mass only. Third, the negative capacitance itself is used to reduce the stiffness of the absorber in order to change the passive tuning frequency toward lower values.

After a brief description of the applied semi-passive and -active techniques in Sect. 2, the key aspects of Sect. 3 are the design process including the geometry optimization of the absorber and piezoelectric elements, to maximize the electromechanical coupling, as well as the derivation and experimental validation of a simplified analytical model of the coupled system. Section 4 describes the application of the different shunting techniques onto the absorber before ending with a conclusion in Sect. 5.

2 Semi-passive and semi-active techniques

The current trend for the lightweight design of technical structures necessarily brings vibration problems into focus. Passive methods, which are usually effective in a broad frequency range, often are related to a high amount of additional masses to the system. Active vibration control, on the other hand, can efficiently reduce vibrations, but there is always the need for actuation power and a relatively high demand for computational controller performance. The semi-passive and semi-active methods, which have been introduced in the last decades, are situated between the passive and active techniques of vibration control, regarding their costs and the technical complexity. A semi-passive system does not need additional power for actuation or the computation of sensory signals. It rather makes use of the ability of electromechanical transducers, such as piezoelectric elements, to convert mechanical energy into electrical and vice versa. The transducers are connected to electrical circuits to change the mechanical behavior of the host structure. Most of these techniques have a rather narrowband effectiveness. Because of this, their potential can be exploited most, on structures which have also a distinctive resonant vibration characteristic.

In the context of this article, a semi-passive system is defined as a system, where only external energy is needed to supply electric components, such as operational amplifiers. Semi-active systems, on the other

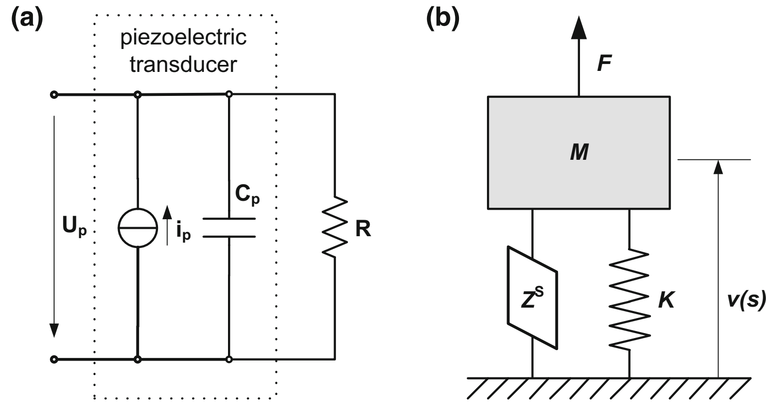

Fig. 1 Principle of an R-shunted mechanical system. **a** Electric circuit consisting of a piezoelectric element and an R-shunt. **b** Mechanical model of a 1-DOF oscillator with a general shunt impedance

hand, directly transmit external energy in form of actuation forces to the host structure, still without the need of sensors. In the following, the basic concepts, which are used for the tuning of a vibration absorber, are described.

2.1 R-shunt

The most basic electrical circuit to reduce vibrations with a shunted system is the purely passive resistive shunt (R-shunt). It has been introduced already in 1991 by [6]. A simple resistor is connected between the terminals of the piezoelectric element which is bonded to a host structure. The mechanical energy is transformed by the transducer into electrical energy and dissipated inside the ohmic resistance. Figure 1a shows the principle scheme of the resistive shunt circuit connected to a piezoelectric element, which is simplified as a capacitance and a current source. Figure 1b shows the mechanical model of a mechanically undamped, single degree of freedom oscillator that is shunted to an electrical impedance.

The admittance of an arbitrarily shunted mechanical system in the Laplace domain is described by Eq. (1), wherein the relation of the velocity $\boldsymbol{v}$ to force $\boldsymbol{F}$ is defined by the modal mass $\boldsymbol{M}$, modal stiffness $\boldsymbol{K}$, and the impedance contribution $\boldsymbol{Z}_{jj}^{\mathrm{S}}$ of the shunt:

$$\frac{\boldsymbol{v}(s)}{\boldsymbol{F}(s)} = \frac{1}{\boldsymbol{M}s + \frac{\boldsymbol{K}}{s} + \boldsymbol{Z}_{jj}^{\mathrm{S}}(s)} \tag{1}$$

The mechanical impedance $\boldsymbol{Z}_{jj}^{\mathrm{S}}$ is defined as the product of the mechanical impedance of the open circuit piezoelectric $\boldsymbol{Z}_{jj}^{\mathrm{D}}$ and the non-dimensional description of the mechanical impedance of the shunt $\overline{\boldsymbol{Z}_{jj}^{\mathrm{S}}}$ by [6] through Eqs. (2)–(4)

$$\boldsymbol{Z}_{jj}^{\mathrm{S}}(s) = \boldsymbol{Z}_{jj}^{\mathrm{D}}(s) \cdot \overline{\boldsymbol{Z}_{jj}^{\mathrm{S}}}(s) \tag{2}$$

$$\boldsymbol{Z}_{jj}^{\mathrm{D}}(s) = (1/s)\boldsymbol{K}_{jj}^{\mathrm{E}} - \frac{1}{1 - \boldsymbol{k}_{ij}^{2}} \tag{3}$$

with $\boldsymbol{K}_{jj}^{\mathrm{E}}$ as the mechanical stiffness of the piezoelectric element with shorted electrodes and $\boldsymbol{k}_{ij}$ as the piezo material electromechanical coupling factor.

$$\overline{\boldsymbol{Z}_{jj}^{\mathrm{S}}}(s) = \overline{\boldsymbol{Z}_{jj}^{\mathrm{R}}}(s) = 1 - \frac{\boldsymbol{k}_{ij}^{2}}{1 + RC_{pi}^{\mathrm{S}}s} \tag{4}$$

with

$_i$ = index denoting the ith direction of the electrical field
$_j$ = index denoting the jth direction of the mechanical effect

C_{pi}^{S} = inherent capacitance of the piezoelectric shunted in the ith direction at constant strain (clamped)
R = ohmic resistance of the shunt.

For the better physical understanding, Eq. (5) gives the definition of the later on discussed generalized electromechanical coupling coefficient, which is related to the amount of energy that can be transformed from the coupled mechanical system to the electrical circuit and vice versa [6].

$$\boldsymbol{K}_{ij}^{2} = \frac{\boldsymbol{K}_{jj}^{E}}{\boldsymbol{K} + \boldsymbol{K}_{jj}^{E}} \cdot \frac{\boldsymbol{k}_{ij}^{2}}{1 - \boldsymbol{k}_{ij}^{2}} \tag{5}$$

An analysis of Eq. (4) shows, that when R is zero, which is the short circuit configuration, there are no accumulated electric charges between the terminals and therefore no extra stiffness is generated by the piezoelectric element. At that configuration, the electromechanical system has its lowest Eigenfrequency. When R starts to increase, current starts to flow and electrical energy is dissipated, thus damping is added to the system. There is an optimal point where the maximum energy is dissipated. Analytical equations for the optimal values of an R-shunt were first presented in [6] and later extended by [8]. Equation (6) gives the resistance value when the mechanical displacement of the mass $\boldsymbol{M}$ is minimized.

$$R_{\text{R-opt}} = \frac{2}{C_{pi}^{S}\omega_{n}^{E}} \sqrt{\frac{1}{4 + 2\boldsymbol{K}_{ij}^{2}}} \tag{6}$$

In this case, ω_{n}^{E} is the mechanical Eigenfrequency of a 1-DOF system with the piezoelectric element short circuited. If R increases further, the current flowing through the piezo starts to decrease, since the generated voltage is limited, and the circuit tends to the open circuit configuration, which has the highest stiffness generated by the piezoelectric transducer and therefore the highest Eigenfrequency. This technique is used in Subsect. 4.1 in order to change the damping of the tuned mass absorber.

2.2 RL-shunt

An expansion of the R-shunt is the resistive resonant shunt (RL-shunt), which has also been described thoroughly by [6] and was originally introduced by [10]. In this case, an additional inductor is connected to the piezoceramic and the resistor. The resultant RLC-circuit is a damped resonant system, which can be tuned through a change of inductance to a certain frequency, e.g., the mechanical Eigenfrequency of the mechanical system, and therefore acts similar to a tuned mass absorber itself. Since the impedance is low at the electrical resonance frequency, high currents are flowing through the circuit, leading to an increased energy dissipation and thus to a higher level of damping of the host structure, compared to the R-shunt. With a very low resistance value, the system behaves like an L-shunt and without any energy dissipation. The system is then equal to an undamped absorber and the two characteristic poles around the absorption frequency can be noted. By varying the inductance value, two characteristic fixpoints whose amplitudes are independent from damping values can be equalized [8,11]. As the resistance increases, these Eigenmodes are getting damped, and the amplitudes of vibration decrease until an optimum is achieved. If the resistance continues to increase, the electric circuit behaves as over-damped, and the electrical oscillation is oppressed. The structural Eigenfrequency then tends toward the open circuit Eigenfrequency (when $R \to \infty$) of the coupled system. The maximum possible attenuation level using this method is highly dependent on the generalized electromechanical coupling coefficient, which describes the amount of energy that can be transferred from the mechanical to the electrical system. It is limited by the geometry and material boundary conditions.

The principle of an RL-shunted piezoelectric transducer is shown in Fig. 2. The transducer is again simplified as a capacitance and a current source, the shunt consists of a resistor and an inductor. The non-dimensional mechanical impedance for the RL-shunt, which can be substituted analogously to the R-shunt into Eq. (2), is given by Eq. (7) and derives from [6]:

$$\overline{\boldsymbol{Z}_{jj}^{S}}(s) = \overline{\boldsymbol{Z}_{jj}^{RL}}(s) = 1 - \boldsymbol{k}_{ij}^{2} \left(\frac{\left(\frac{\omega_e}{\omega_n}\right)^2}{\gamma^2 + \gamma R C_{pi}^{S} \omega_{n}^{E} \left(\frac{\omega_e}{\omega_n}\right)^2 + \left(\frac{\omega_e}{\omega_n}\right)^2} \right) \tag{7}$$

with

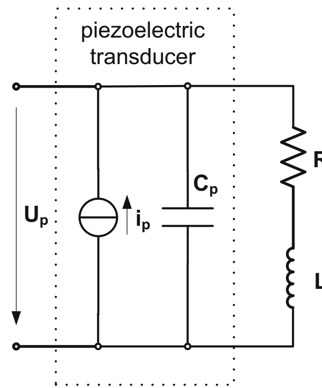

Fig. 2 Electric oscillator circuit consisting of a piezoelectric element and a series RL-shunt

$\gamma = s/\omega_n^{\mathrm{E}}$ = non-dimensional frequency
ω_n^{E} = mechanical Eigenfrequency of the 1-DOF system with the piezoelectric element short circuited
ω_e = electrical Eigenfrequency of the RL-shunted piezoelectric element
ω_n = mechanical Eigenfrequency of the 1-DOF system.

Regarding technical applications, the capacitance value of the applied piezoelectric element is in the range of some nF to µF. For low Eigenfrequencies of the mechanical system, the needed inductance values can be very high, maybe tens or hundreds of Henry. At that scale, a regular coil inductor would have large dimensions and masses, which are both not desirable. For that reason, a widely used layout for a synthetic impedance, which is described in [12], can be used: a gyrator circuit inverts the impedance of a passive element present in the circuit. Because this circuit needs supply power, the RL-shunt with a synthetic inductance is a semi-passive technique. When adequately designed, an RL-shunted system using Antoniou's circuit is always stable. Only when modifying the circuit, which can be unintentionally the case, when using operational amplifiers with additional internal functionalities, like current limiters, a negative real part of the electrical impedance might be generated, which can destabilize the system. Analytical equations for the optimal values of a RL-shunt were first presented in [6] and later extended by [8]. Equation (8) gives the resistance value when the mechanical displacement of mass $\boldsymbol{M}$ is minimized. Equation (9) gives the optimal inductance value.

$$R_{\text{RL-opt}} = \frac{2}{C_{pi}^{\mathrm{S}}\omega_n^{\mathrm{E}}}\sqrt{\frac{1}{\frac{2}{\boldsymbol{K}_{ij}^2} + 4 + 2\boldsymbol{K}_{ij}^2}} \tag{8}$$

$$L_{\text{RL-opt}} = \frac{1}{C_{pi}^{\mathrm{S}}(\omega_n^{\mathrm{E}})^2}\frac{1}{1+\boldsymbol{K}_{ij}^2} \tag{9}$$

The RL-shunt is used in Subsect. 4.2 to reduce the absorption effect of a tuned mass absorber.

2.3 Negative C-shunt

A piezoelectric material electrically has a capacitive behavior, since there is an unbalance of electric charges between its terminals when a voltage appears (caused by mechanical stress). Reciprocally, the mechanical effect of the unbalanced electric charges is an increase in stiffness. In order to lower this mechanical stiffening, [13] patented a system with a negative capacitance connected to the piezoelectric element. In [14], the authors tested different negative C-shunt circuits for the application of this approach e.g., in order to change the stiffness of a PVDF material. In [15], a similar circuit is used in series with a resistance. Figure 3 shows the principle scheme of a negative C-shunted piezoelectric element.

Unfortunately, the presently only known passive components that exhibit the behavior of a negative capacitance are semiconducting materials. As discussed by [16], semiconductor diodes can reach values in the lower nF range. Since the technically needed range for the given purpose lies above these limits, such a capacitance has to be obtained using a synthetic impedance circuit based on an operational amplifier. This so-called negative impedance converter (NIC) inverts the signal of a passive element in the circuit, as can be seen in Fig. 4.

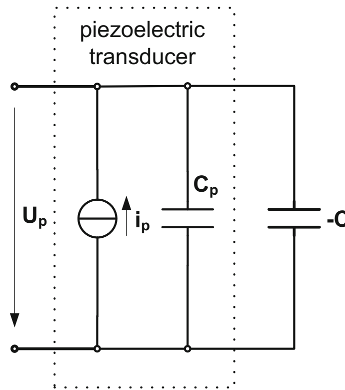

Fig. 3 Electric circuit consisting of a piezoelectric element and a negative C-shunt

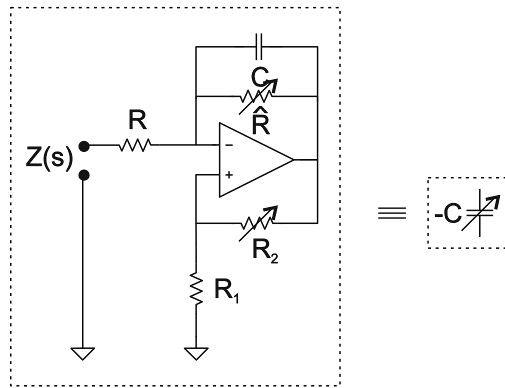

Fig. 4 Variable negative capacitance circuit

Considering an ideal operational amplifier, it can be assumed that the impedance at the terminals is described by Eq. (10), when a limited frequency band and a limited range of amplitude are considered.

$$Z(s) = -\frac{R_1}{R_2}\frac{1}{Cs} \tag{10}$$

This electronic circuit can also be considered as a closed-loop controller, where the effects of feedback (in this case, positive and negative) and of the operational amplifier's parameters must be well understood in order to achieve good performance. Since such a negative capacitance circuit can introduce forces into the system, deriving from the operational amplifier supply power, such a system is a semi-active one. The circuit values must be chosen in a certain way to obtain stability for the complete electromechanical system [17]. In order to obtain a tunable negative capacitance controller, R_2 was chosen to be variable. Out of damping performance reasons, that are further explained in Sect. 4.3, $\widehat{R}$ is also variable, while all other circuit values can remain fixed. According to [8], it can be analytically derived that the resonance frequency of the system is:

$$\omega_{res} = \omega_n^{\mathrm{E}}\sqrt{\frac{1+\delta+\delta\boldsymbol{K}_{ij}^2}{1+\delta}} \tag{11}$$

wherein δ is defined as the ratio between the capacitance of the piezoelectric element and the negative capacitance connected:

$$\delta = \frac{C_{pi}^{\mathrm{S}}}{C} \tag{12}$$

When the absolute value of the negative capacitance tends to the capacitance of the piezo element, the system becomes very sensitive and the resonance frequency can be drastically changed. At some point, the system

becomes unstable, so the actual Eigenfrequency cannot be reduced to zero. Using the Hurwitz criterion, [8] shows that the system is stable if:

$$\delta > \delta_{\text{crit}} = \frac{-1}{1 + \boldsymbol{K}_{ij}^2} \tag{13}$$

Experimental observations have shown that, for low damped systems, it is practically very difficult to reach the theoretical stability boundary. Considering a safety margin β between the real and the theoretical stability limit, δ'_{crit} can be rewritten:

$$\delta'_{\text{crit}} = \frac{-\beta}{1 + \boldsymbol{K}_{ij}^2} \tag{14}$$

The critical resonance frequency attainable by the system can then be analytically calculated by substituting Eq. (14) into Eq. (11) leading to:

$$\omega_{\text{crit}} = \omega_n^{\text{E}} \sqrt{\frac{1 + \boldsymbol{K}_{ij}^2}{1 + \frac{1}{1-\beta} \boldsymbol{K}_{ij}^2}} \tag{15}$$

The negative C-shunt is used in Subsect. 4.3 to change the Eigenfrequency of an absorber.

2.4 RLC-shunt

As mentioned above, the generalized electromechanical coupling coefficient, which is among other factors limited by the geometry, determines the amount of energy, which can be transferred from the mechanical to the electrical system and vice versa. This leads directly to a relation between, e.g., the dimension and mass of the used transducers and the performance of an RL-shunted system. In order to artificially increase this coupling, [11] introduced an additional negative capacitance in series and parallel to the RL-shunt. Figure 5 shows the simplified scheme of an RLC-circuit, wherein the series negative capacitance can be realized with a circuit shown in Fig. 4.

When the series negative capacitance is connected to the mechanical system, it behaves as a spring element with a negative stiffness, thus it reduces the Eigenfrequency of the system and leads to an apparent increase of the generalized electromechanical coupling coefficient. With rising negative capacitance values, the two arising poles, characteristic for the absorption effect of the RL-shunt, spread away from each other regarding their frequency values. This is equivalent to increasing the oscillating masses of a tuned vibration absorber. Again, an optimal value for the resistor regarding the mechanical vibration attenuation can be calculated [8,11]. Equation (16) gives the optimal value for the ratio δ, in order to minimize the mechanical displacement. Equation (17) to (19) give, respectively, the optimal resistance, inductance, and negative capacitance values.

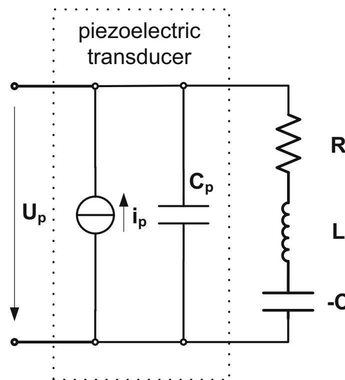

Fig. 5 Electric oscillator circuit consisting of a piezoelectric element and a series RLC-shunt

$$\delta_{\text{opt}} = \frac{1.1135 \cdot \boldsymbol{K}_{ij}^2 - 1}{\boldsymbol{K}_{ij}^2 + 1} \tag{16}$$

$$R_{\text{RLC-opt}} = \sqrt{1 + \delta_{\text{opt}}} R_{\text{RL-opt}} \tag{17}$$

$$L_{\text{RLC-opt}} = (1 + \delta_{\text{opt}}) L_{\text{RL-opt}} \tag{18}$$

$$C_{\text{RLC-opt}} = C_{pi}^{\text{S}} / \delta_{\text{opt}} \tag{19}$$

The main advantage of the RLC-shunt compared to the RL-shunt is that the maximum attenuation depends little on the generalized electromechanical coupling coefficient. At this point, the negative capacitance must be correctly tuned, otherwise the system can be destabilized. Depending on the circuit type and host structure, the values for the negative capacitance are limited [9]. This type of shunt is used in Subsect. 4.2 to minimize the absorption effect of a tuned mass absorber.

3 Design of a shunted vibration absorber

The tuned mass absorber used in this study consists of a 2 × 2 twill woven 8 symmetrical layered carbon fiber beam (5 × 35 × 275 mm). A vertical force excites the system at its middle clamp (35 × 35 mm) and is measured together with the acceleration at this point with an impedance sensor. At both ends, masses are attached (2 × 0.2 kg), whose accelerations are measured with accelerometers. Bonded to the upper and lower surfaces of the beam there are piezoelectric ceramic patches, which are all connected in parallel and to one shunt circuit. The dimensions of the piezoelectric patches are optimized numerically. A side view of the absorber is depicted in Fig. 6.

3.1 Numerical design

A finite element (FE) model has been set up with the commercial software ANSYS. The carbon fiber beam is modeled using three dimensional 20-node non-linear solid elements. Since the layers of the composite material can be considered to be homogeneous and elastically linear, the material is modeled as orthotropic. Some initial material characteristics are provided by the manufacturer, like the in-plane elastic moduli ($E_{0^\circ} = E_{90^\circ} = 60$ GPa) and the Poisson's ration ($\nu = 0.3$). However, in order to fit the first six experimentally identified Eigenfrequencies, an optimization was carried out to adjust the full matrix of the orthotropic material property. The resultant material property is shown in Table 1.

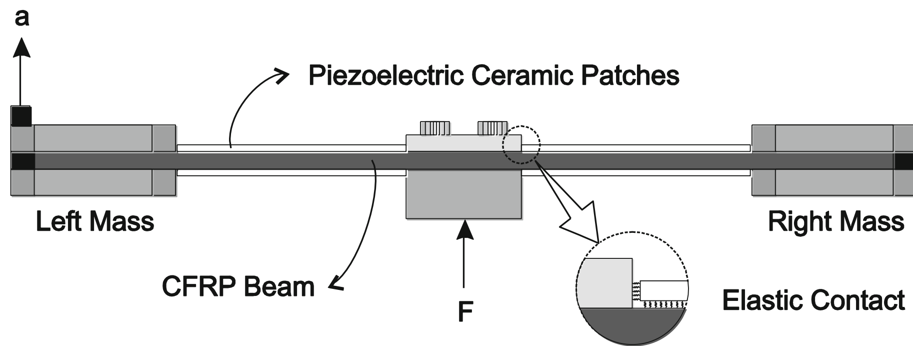

Fig. 6 Tuned mass absorber

Table 1 Material parameters

Young's modulus (GPa)	Shear modulus (GPa)	Poisson's ratio
$E_x = 68{,}021$	$\tau_{xy} = 2{,}654$	$\nu_{xy} = 0{,}0363$
$E_y = 57{,}500$	$\tau_{xz} = 4{,}425$	$\nu_{xz} = 0{,}3147$
$E_z = 7{,}500$	$\tau_{yz} = 3{,}406$	$\nu_{yz} = 0{,}0421$

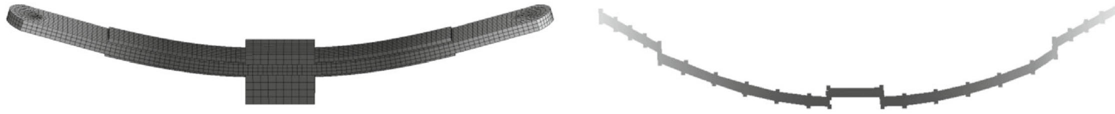

Fig. 7 1st bending mode of the finite element model (*left*) and the experimental modal analysis (*right*) at 167 Hz

This study is mainly interested in the first symmetrical vertical bending mode, which was calculated numerically and experimentally identified using a Polytec scanning laser vibrometer and the poly-reference least squares complex frequency domain algorithm. The modeshapes of both methods are depicted in Fig. 7. The clamp at the middle is modeled with three dimensional 20-node non-linear solid elements with isotropic material properties. The attached masses are added as lumped elements elastically connected to the beam at the corresponding surface, which allows a local deformation. The ceramics are modeled as piezoelectric elements, where the compliance, strain, and permittivity full matrices are provided by the manufacturer. All patches are polarized in the vertical direction, and the surfaces connected to the CFRP beam are electrically grounded. The optimal piezoceramics configuration is analyzed, in order to maximize the generalized electromechanical coupling coefficient ($\boldsymbol{K}_{31}$). ANSYS standard optimal-space filling design of experiments is used together with a neural network response surface. Different piezoceramic materials, bonding conditions, and number of patches are tested. The dimensions of the patches are varied, and the optimization is carried on. The thickness of the piezoceramic is the most sensitive parameter, and a global optimum is found when using four patches and bonding all of them to the beam and next to the clamp at the middle. The optimized dimensions are then compared to the manufacturer's standard sizes and four patches of $2 \times 25 \times 70$ mm each are chosen. The maximized calculated value of $\boldsymbol{K}_{31}$ is found to be 0.35. At this stage of the design process, the prototype is built. Afterward, the FE model is updated in order to better represent the results obtained from the experimental analyses and validate the modeling approach that is shown in the following subsection. Therefore, an elastic bonding coefficient is modeled between the piezoceramics and the contact surfaces, leading to an experimentally validated generalized electromechanical coupling coefficient $\boldsymbol{K}_{31}$ of 0.26. An optimization is performed to fit experimental open (f_{d}) and short (f_{e}) circuit Eigenfrequencies, by varying the bonding coefficients. The comparatively lower value of $\boldsymbol{K}_{31}$ can be explained by the fact that the real glue used to bond the patches is not an ideal connection, since it might not transmit all the mechanical strain. That means the conversion between mechanical and electric energy is attenuated.

3.2 Analytical calculation

The fitted FE model is then reduced and imported in Matlab. Based on the single degree of freedom equation of motion that has been analytically derived in [8], a 2-DOF system is presented that takes the mass at the base of the absorber into account. The equation of motion describes both electrical and mechanical parts of the system.

A mass M represents the mass at the base, and another mass m stands for an equivalent vibrating mass of the CFRP beam, piezoceramic transducers, and tip masses. Considering a forced vibration of a mass M connected to another mass m through a spring (c_0), a damper (d_0), and a piezoelectric element, which has also a mechanical stiffness (c_p), the mechanical equations of the masses read:

$$\begin{aligned} M\ddot{x}_2 - d_0\,(\dot{x}_1 - \dot{x}_2) - c_0(x_1 - x_2) - F_p = F \\ m\ddot{x}_1 + d_0\,(\dot{x}_1 - \dot{x}_2) + c_0\,(x_1 - x_2) + F_p = 0 \end{aligned} \tag{20}$$

Here, the mechanical damping between the two masses of the system, including the transducers, is represented by a single parameter d_0, which will be experimentally obtained later. A possible damping and stiffness between the base mass and the ground is neglected in the equations, because the aim was not to include the behavior of a real host structure for the absorber. Furthermore, F_p is the force generated by the piezoelectric element, which can be derived from the constitutive electromechanical equations of a linear piezoelectric material:

$$F_p = c_p(x_1 - x_2) - c_p d_p u_p \tag{21}$$

where u_p is the voltage generated by the piezoelectric element, and d_p is the charge density per unit stress of the electromechanical system, as defined by [8], which can be obtained using:

$$d_p = \frac{1}{c_p}\sqrt{\boldsymbol{K}_{ij}^2 C_{pi}^{\mathrm{S}}(c_p + c_0)} \tag{22}$$

In the given case, $\boldsymbol{K}_{ij}$ corresponds to $\boldsymbol{K}_{31}$ of the first bending mode of the clamped absorber. Electrically, the piezoelectric material behaves as a current source with an internal capacitance (C_{pi}^S), as seen in Fig. 5. More precisely, an internal electrical resistance in the piezoelectric material (R_{pi}^S) is also modeled. The electric current generated by the transducer can be calculated by:

$$i_p = -c_p d_p\,(\dot{x}_1 - \dot{x}_2) \tag{23}$$

The piezoelectric element is externally connected to a series RLC network, whose equation can be derived using Kirchhoff's second law and the constitutive equations for RLC elements:

$$u_p = L\frac{di_{\mathrm{ext}}}{dt} + Ri_{\mathrm{ext}} + \frac{1}{C}\int i_{\mathrm{ext}}dt \tag{24}$$

More generally, the external network connected to the transducer can be represented by an electrical impedance in the Laplace domain $Z_{\mathrm{ext}}(s)$, as seen in Eq. (25).

$$U_p\,(\mathrm{s}) = \left(Ls + R + \frac{1}{Cs}\right) I_{\mathrm{ext}}\,(s) = Z_{\mathrm{ext}}(s) I_{\mathrm{ext}}(s) \tag{25}$$

Now, if the external network (RLC-series) is connected in parallel to the internal circuit of the transducer (RC-series), the equivalent impedance $Z_{eq}\,(s)$ seen by the internal current source of the transducer can be represented by the following equation:

$$\frac{1}{Z_{eq}(s)} = \frac{1}{Z_{\mathrm{ext}}(s)} + \frac{1}{R_{pi}^{\mathrm{S}} + \frac{1}{C_{pi}^{\mathrm{S}} s}} \tag{26}$$

Here, R_{pi}^{S} defines the inner resistance of the piezo element and Z_{ext} the impedance of the external network. When combining Eq. (23) and Eq. (26), it is possible to obtain the final voltage generated by the transducer:

$$U_p\,(\mathrm{s}) = Z_{eq}\,(s)\,I_p\,(s) = -Z_{eq}\,(s)\,c_p d_p (X_1 - X_2)s \tag{27}$$

Considering the displacement X_1 of the mass m, X_2 of the mass M, and the voltage U_p as variables in the Laplace domain, substituting Eq. (21) into Eq. (20) and using Eq. (27), the dynamic behavior of the system is given by the following equation of motion:

$$\begin{bmatrix} m & 0 & 0 \\ 0 & M & 0 \\ 0 & 0 & 0 \end{bmatrix} \begin{bmatrix} X_1 \\ X_2 \\ U_p \end{bmatrix} \mathrm{s}^2 + \begin{bmatrix} d_0 & -d_0 & 0 \\ -d_0 & d_0 & 0 \\ c_p d_p Z_{eq} & -c_p d_p Z_{eq} & 0 \end{bmatrix} \begin{bmatrix} X_1 \\ X_2 \\ U_p \end{bmatrix} \mathrm{s} + \begin{bmatrix} c_0 + c_p & -c_0 - c_p & -c_p d_p \\ -c_0 - c_p & c_0 + c_p & c_p d_p \\ 0 & 0 & 1 \end{bmatrix} \begin{bmatrix} X_1 \\ X_2 \\ U_p \end{bmatrix} = \begin{bmatrix} 0 \\ F \\ 0 \end{bmatrix} \tag{28}$$

Finally, Eqs. (24, 28) allows a frequency response function (FRF) calculation of the reduced model. A final optimization is carried out in order to adjust the reduced model by fitting the calculated and experimental FRF. A derivative-free method is used to minimize the RMS error between the calculated and experimental responses. This model is then used for all analyses of its shunt damping and tuning capabilities using different shunt circuits.

3.3 Experimental validation of the simplified model

An experimental modal analysis using a first prototype is made in order to fit the carbon fiber properties, before the piezoceramics were bonded to the beam. Afterward, when the geometric optimization is completed, the piezoceramics are added. The inherent capacitance (C_{pi}^{S}) and series resistance (R_{pi}^{S}) of the piezoelectric elements are obtained experimentally, since it is a sensitive parameter for the shunt design. A precision spectral impedance analyzer is used for that purpose. The electrical properties of the piezoelectric elements are measured, when already bonded to the structure, and the value is selected at a frequency above a mechanical resonance. Here, the phase of the electrical impedance is close to the ideal minus 90 degrees. The resistance, on the other hand, is measured at high frequency (1 kHz). The reduced analytical model is finally validated by two experimental FRFs, with open and short circuit configuration. The measured FRF is chosen to be the dynamic mass, that is, input force of an electrodynamical shaker at the middle clamp over output acceleration at the base mass. The simulated and experimental dynamic masses are presented in Fig. 8. The amplitude of the response has a value of 33.8 dB and the damping ratio of the absorber is around 0.5 %. Tables 2 and 3 summarize the main characteristics of the mechanical system and the single degree of freedom model.

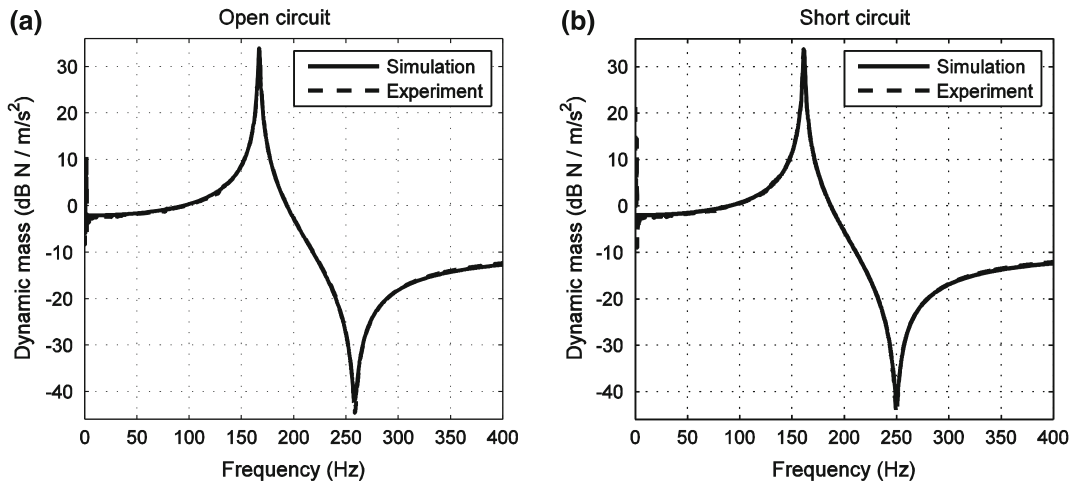

Fig. 8 Dynamic mass at open (**a**) and short (**b**) circuit, simulation (*straight line*) and experiment (*dashed line*)

Table 2 Measured tuned mass absorber characteristics

Description	Symbol	Value
Open circuit mode (Hz)	f_d	167.0
Short circuit mode (Hz)	f_e	161.3
Generalized electromechanical coupling coefficient	K_{31}	0.26
Piezos capacitance (nF)	C_{pi}^{S}	70
Piezos resistance (Ω)	R_{pi}^{S}	55

Table 3 Model parameters

Description	Symbol	Value
Tip mass (kg)	m	0.460
Middle mass (kg)	M	0.329
Eq. stiffness (kN/mm)	$c_p + c_0$	0.474
Damping coefficient (Ns/m)	d_0	4.430
Charge density per stress (m/V)	d_p	0.048

In order to further validate the model regarding the electric properties, the voltage generated by the piezoelectric patches at the open circuit configuration is calculated and experimentally measured. Figure 9 compares both responses and gives evidence of the quality of the model. At the peak frequency, the calculated value is 54.6 V, whereas the measured one is 65.3 V; a difference of approximately 20 %. At the frequency of interest (167 Hz), the calculated value is 1,334 V, whereas the measured one is 1,364 V; a difference of approximately 2 %. This shows that the model sufficiently describes the absorber's electromechanical coupling at the absorption frequency. The peak at around 260 Hz, on the contrary, is not modeled very precisely, but this is only of little interest regarding the application, since its frequency and amplitude strongly depends on the host structure, which is only very rudimentarily comprised with the base mass in the equation.

The measurement devices used for the experimentally measured FRF consist of an electrodynamic shaker, used as the vibration source, an impedance sensor which is mounted in between the absorber and the shaker and accelerometers on the tip of the absorber's beams. Acceleration, force, and voltage are measured by an FFT analyzer. The experimental setup can be seen in Fig. 10a. Figure 10b shows the configurable electronic board consisting of different shunts. With a DIP switch (dual in-line package switch) all of the shunt circuits described in Sect. 2 can be realized. Depending on the switch positions, the several components, which are a resistor, a synthetic inductance and two kinds of negative capacitances are connected or bridged individually. The board was designed as a laboratory test board with the aim to provide a customizable behavior regarding several aspects: The series resistance (R-shunt) is a variable potentiometer. The synthetic inductance, which is designed in Antonious' gyrator layout [12], is configurable by using another three potentiometers to influence the working point. Finally, the two implemented negative capacitance circuits, from which in the given context only the scheme shown in Fig. 4 was used, can be adjusted by varying the values for R_2 and $\widehat{R}$.

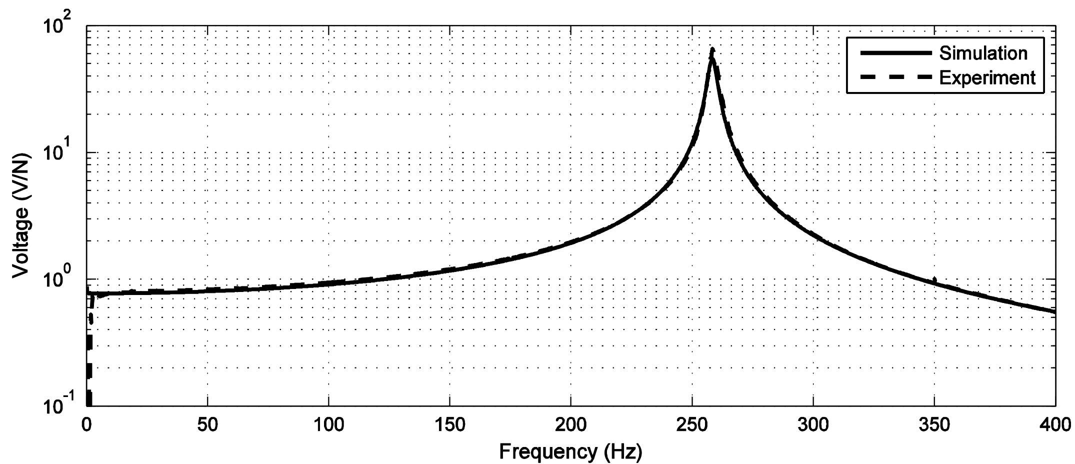

Fig. 9 Open circuit voltage per applied force, simulation (*straight line*) and experiment (*dashed line*)

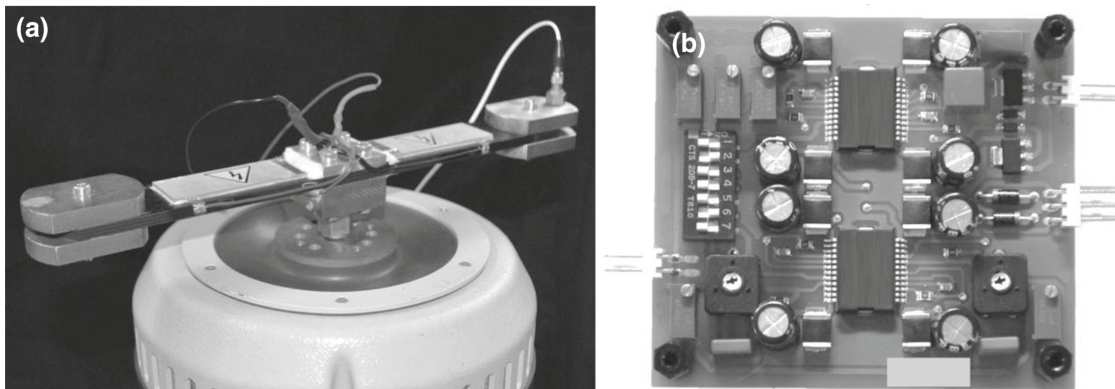

Fig. 10 Experimental setup (**a**) and shunt circuit board (**b**)

In order to provide sufficient information about the experimentally achieved shunt impedances and to allow the reproducibility of the tests, without going into the details of the electronics' development, in the following section only the resultant values for a series resistance, inductance, and capacitance will be listed. These values were obtained through measurements with a precision spectral impedance analyzer.

4 Shunting of the vibration absorber

4.1 R-shunted vibration absorber

In order to change the damping characteristics of the absorber, a simple resistive shunt was applied. Different values of resistances were simulated and tested. Figure 11 shows how an R-shunt affects the dynamic mass behavior. The black line represents the short circuit configuration and the shaded lines, from dark to bright, represent increasing resistance values of the shunt. Table 4 sums up the different results. Since this is a simple passive shunt and no operational amplifier circuits are involved, measurements are in good agreement with calculation.

To further increase the damping of the absorber, it is possible to add a negative capacitance in series to the resistor. This would lead to higher damping values while concurrently lowering the stiffening effect of the R-shunt. The unwanted shift of Eigenfrequency of the R-shunt which can be observed could then be compensated.

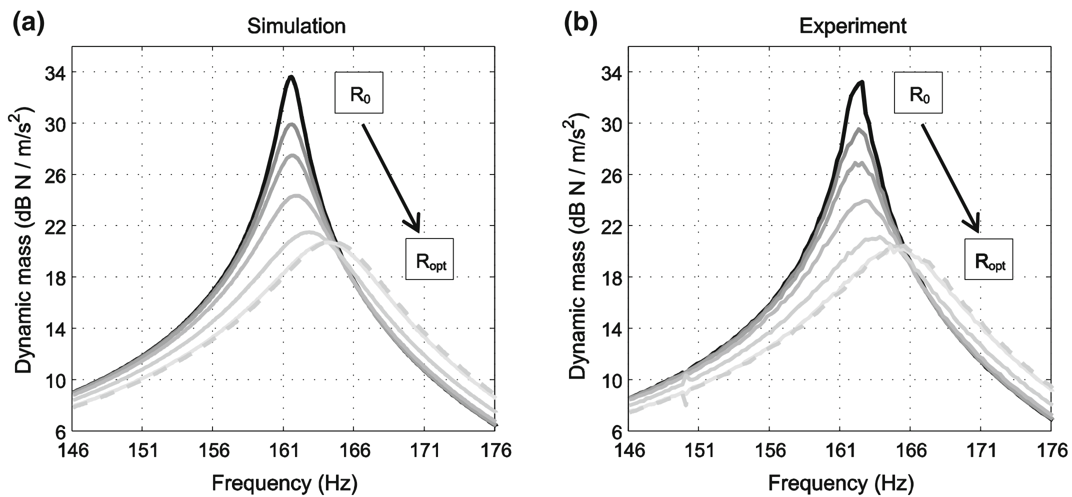

Fig. 11 Dynamic mass at short circuit (*black solid line*), with increasing resistances (R_0 to R_{opt} are increasing with brightness) and with resistance R_5 beyond the optimum (*dashed line*), simulation (**a**) and experiment (**b**)

Table 4 R-shunt characteristics

	Value (kΩ)	Attenuation (dB)		Eigenfreq. (Hz)	Damp. Ratio (%)
		Sim.	Exp.		
R_0	0.00	0.00	0.00	161.3	0.48
R_1	1.00	−3.50	−3.72	161.3	0.73
R_2	2.00	−6.12	−6.28	161.3	0.96
R_3	4.00	−9.25	−9.32	161.7	1.39
R_4	8.00	−12.1	−12.1	162.6	1.95
R_{opt}	13.8	−12.9	−13.0	164.0	2.14
R_5	15.0	−12.8	−12.8	164.2	2.13

4.2 RLC-shunted vibration absorber

For some technical applications of tuned mass absorbers, it can be useful to temporarily reduce the effect of the absorber, e.g., for subjective evaluations of vibrational countermeasures. Active vibration control systems can simply be activated or deactivated for a direct comparison of their effectiveness, on the contrary passive absorber systems have to be demounted, retuned, and remounted again. This makes it more difficult for test persons to judge the systems subjective performance. To overcome this problem, an optimal RL-shunt and an optimal RLC-shunt have been designed and applied to the vibration absorber, thus allowing it to overdampen the absorber characteristics to an extent, where the absorber system behaves almost as an additional mass only, rather than acting as an absorber onto the host structure.

The optimal RL- and RLC-shunt values were obtained using the analytical equations previously described in Sect. 2 and applied to the reduced model of the absorber. Figure 12 shows how the dynamic mass of the mechanical system is influenced by these shunt circuits. The simulation results in Fig. 12 show that an optimal RL-shunt is capable of attenuating 25.0 dB in comparison with the short circuit configuration. The benefit of the negative capacitance is also shown, where the RLC-shunt is capable of attenuating 31.6 dB. When experimentally applying an optimally tuned RL-shunt, there is a peak reduction of 24,5 dB compared to when no shunt is present. An optimally tuned RLC-shunt reduces in the experiment the dynamic mass by 31.2 dB, which confirms the benefit of the negative capacitance.

Table 5 sums up both shunt characteristics. It can be noticed as an extra advantage that the negative capacitance shunt reduces the optimal values needed for the resistor and the inductor. The calculated vibration attenuation of the shunts compared to the short circuit configuration is in good agreement with the measured values.

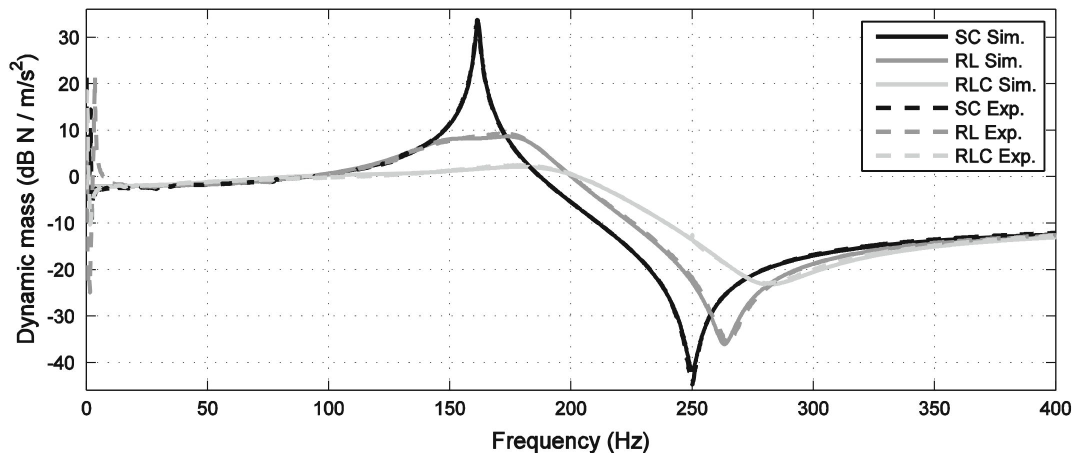

Fig. 12 Dynamic mass at short circuit (*black line*), optimal RL-shunt (*dark gray line*) and optimal RLC-shunt (*light gray line*) configurations, simulation (*solid lines*) and experiment (*dashed lines*)

Table 5 RL and RLC shunt characteristics

	Short circuit	RL-shunt		RLC-shunt	
		Sim.	Exp.	Sim.	Exp.
Resistance (kΩ)	–	4.97		1.83	
Inductance (H)	–	12.9		1.74	
Capacitance (nF)	–	–		−81.7	
Max. amplitude (dB)	33.7	8.72	9.25	2.15	2.47
Attenuation (dB)	–	25.0	24.5	31.6	31.2

4.3 C-shunted vibration absorber

When a capacitance is connected to the piezoelectric transducer, its elasticity is changed, leading to a shift of the mechanical resonance frequency of the absorber. If a positive capacitance is connected, the resonance value can be shifted to any value between short circuit and open circuit Eigenfrequency. If a negative capacitance is connected, according to Eq. (11), it is theoretically possible to adjust the Eigenfrequency of the absorber between the short circuit Eigenfrequency and zero. A calculation using the reduced model shows how different negative capacitance values are capable of changing the Eigenfrequency of the absorber. The results are plotted in Fig. 13. When there is no extra capacitance connected in series (C $\rightarrow \infty$), the system behaves as the short circuit configuration and δ tends to zero, since it is defined as the ratio between C_{pi}^{S} and C. In the given case, the mechanical absorption frequency of the coupled system is 161 Hz. When the negative capacitance increases, the mechanical Eigenfrequency starts to decrease, since the global capacitance of the system is reduced. As the absolute value of the negative capacitance tends toward the capacitance of the piezoelectric element, the resonance frequency of the system becomes very sensitive to minor changes in the negative capacitance value. Between a capacitance ratio δ of -0.90 and -0.93, there is a change in Eigenfrequency from approximately 100 to 40 Hz before the stability limit is reached.

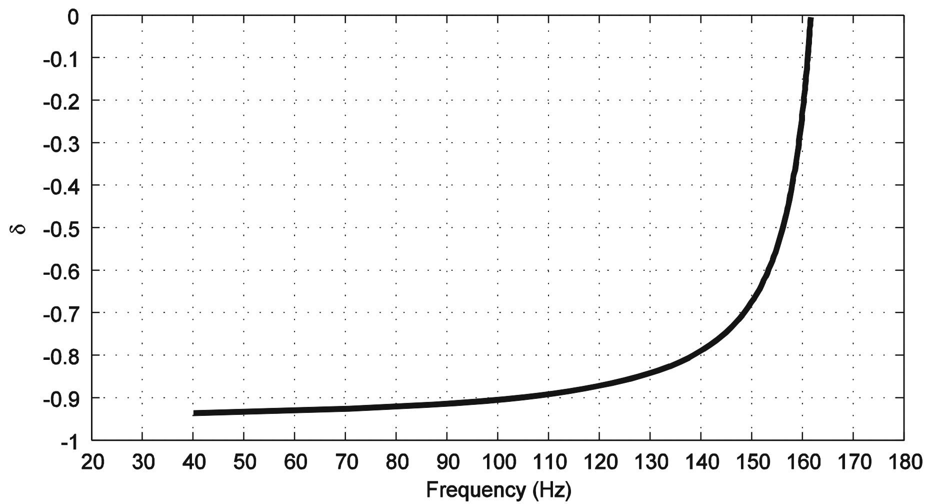

Fig. 13 Calculated absorber resonance frequency versus negative capacitance ($\beta \leq 0.984$)

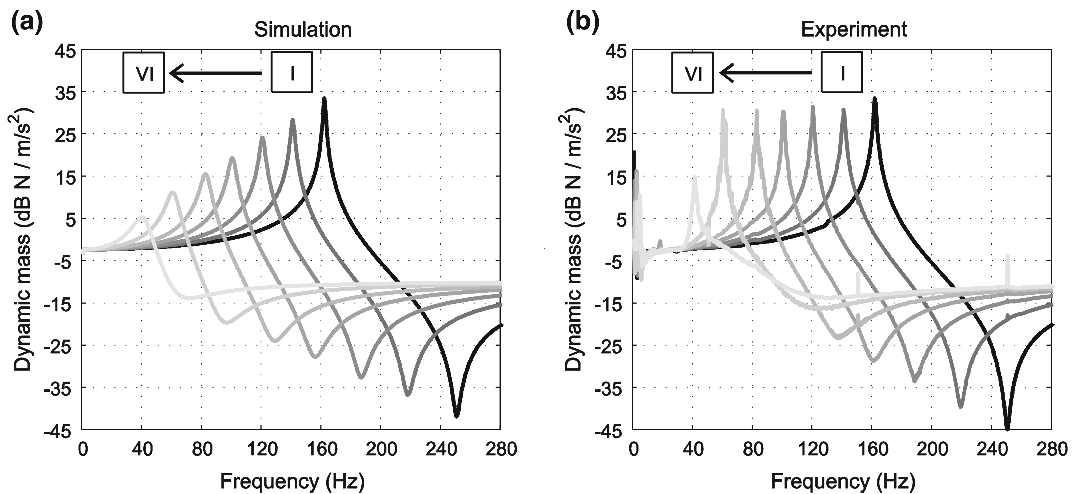

Fig. 14 Dynamic mass at short circuit (*black line*) and with increasing negative capacitance values (*gray lines*) according to Table 6, simulation (**a**) and experiment (**b**)

Table 6 C-shunt characteristics for the idealized negative capacitance

Case	Capacitance			Eigenfreq. (Hz)
	Sim. (nF)	Exp. (nF)	Error (%)	
Short circuit	–	–	–	161.3
I	−90.2	−92.2	2.2	140.4
II	−81.3	−82.8	1.8	120.1
III	−78.4	−79.8	1.8	100.0
IV	−77.1	−78.5	1.9	82.3
V	−76.2	−77.8	2.1	60.5
VI	−75.7	−77.6	2.5	40.5

Following the numerical studies, several negative capacitance values were experimentally tested on the mechanical absorber. The dynamic mass was measured between the shaker excitation and the base of the absorber, and the changes of resonance frequency were observed. Figure 14 depicts the numerical and experimental results. Figure 14a, b show the range of tuning (I–VI). This represents the purely capacitive shunt, where solely the inherent resistance of the piezoelement is present. Starting from the right, the short circuit configuration has the highest resonance frequency. As the negative capacitance increases, the resonance peak is shifted toward lower frequencies.

In order to compare simulation and experiment, the Eigenfrequencies of the simulation were adjusted to match those from the experiment. Thus, there is some difference between the ideally calculated values and the experimentally identified ones. Nevertheless, the calculation fairly predicts the experimentally measured absorption frequency with an error of maximal 2.5 % concerning the capacitance values. This error may derive from a difficulty of measuring it precisely. Table 6 summarizes the measured values for the tuning states and an idealized negative capacitance. One can recognize, that the levels of amplitude at the absorption frequency differ, pointing out that the inner resistances of the circuit are not taken into account properly by the simplified model. The reason for that is that in order to achieve a tunable absorber with a constant damping, the $\widehat{R}$ value of the NIC circuit (see Fig. 4) was adjusted at every tuning point. This influences the series resistance of the circuit and has to be modeled more detailed.

A closer insight into this phenomenon can be attained by extending the description for Z_{ext} in Eq. (26) by the parameters of the electric components. According to [17], the impedance of the used NIC circuit can be written as:

$$Z_{ext}(s) = Z_{NIC}(s) = \frac{Rs + \left(\frac{1}{\widehat{R}C}\right)\left(R - \frac{\widehat{R}R_1}{R_2}\right)}{s + \left(\frac{1}{\widehat{R}C}\right)}. \tag{29}$$

The authors of [17] observed that the stability and the resultant damping of the system is depending on $\widehat{R}$. In the previous tests of Subsect. 4.2 when applying the RLC-shunt, the value of $\widehat{R}$ was constantly 1 MΩ. In that case, when there is a moderate negative capacitance value, apparently the idealized model is capable of representing the circuit's behavior. In the case of the C-shunt and in order to achieve higher tuning ratios, which means to get closer to the stability limit, the NIC configurations require an adjustment of the electric components, especially the values for the resistance $\widehat{R}$. That way, the absorption frequency of the absorber can be tuned to 40.5 Hz, corresponding to 24.3 % of the open circuit Eigenfrequency with a negative capacitance value of −77.6 nF. The safety margin in this case is 1.6 % ($\beta = 0.984$). Until a safety margin of 4.9 % ($\beta = 0.961$) and a negative capacitance value of −77.8 nF, the level of amplitude at the absorption frequency could be kept almost constant. A further increase of the negative capacitance value leads to reduced level as can be seen in Fig. 14b and again in Fig. 15b.

Figure 15a shows the calculated dynamic mass, when including the extended model for the NIC circuit described by Eq. (29). The values of the electric components used during the experiments are listed in Table 7. A comparison of the levels of amplitude at the absorption frequencies shows that experiment and calculation are matching better than with the ideal negative capacitance. Even the decrease of amplitude at the tuning frequency of 40 Hz is predicted quite well.

From the technical point of view, it seems to be advisable to have a controllable component for the resistor $\widehat{R}$ in order to achieve a tunable vibration absorber with low damping characteristics. The stability of the global

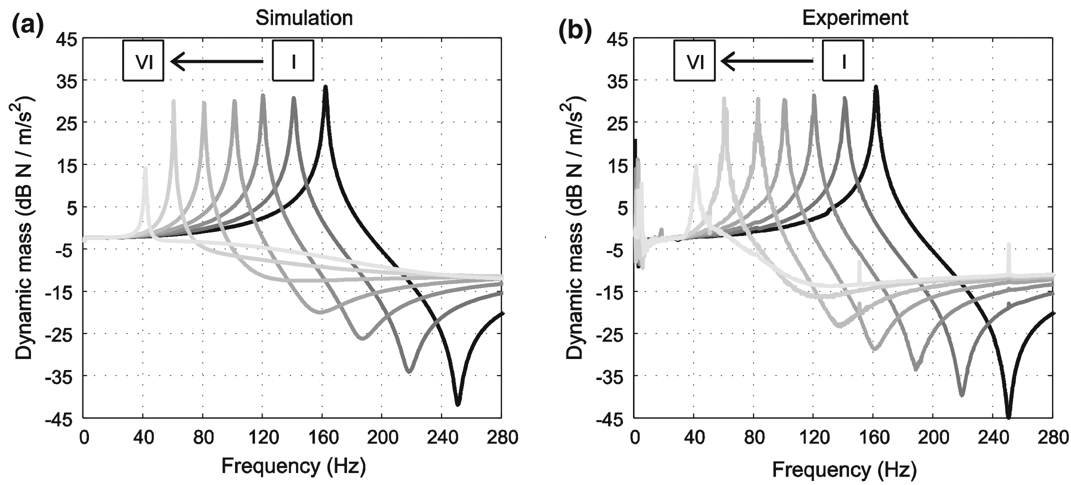

Fig. 15 Dynamic mass at short circuit (*black line*) and with increasing negative capacitance values (*gray lines*) and component parameters according to Table 7, simulation (**a**) and experiment (**b**)

Table 7 Parameters of the C-shunt for the detailed model of a negative capacitance

Case	C (nF)	R (Ω)	R_1(Ω)	R_2(Ω)	$\widehat{R}$(MΩ)	Eigenfreq. (Hz)
Short circuit	–	–	–	–	–	161.3
I	68	132	1,510	2,000	1.41	140.4
II	68	162	1,675	2,000	1.56	120.1
III	68	210	1,735	2,000	1.62	100.0
IV	68	317	1,768	2,000	1.96	82.3
V	68	417	1,786	2,000	2.90	60.5
VI	68	595	1,797	2,000	4.48	40.5

electromechanical system that is connected to the NIC also depends on the voltage and current limits of the operational amplifier. If the voltage generated by the piezoelectric element is higher than the operation voltage of the operational amplifier, it saturates, behaves non-linear, and the system was observed to become unstable. A high voltage NIC has been hence developed, aiming at real life applications, being able to withstand up to ±175V.

5 Conclusion

The present work describes the design process and successful implementation of a tuned mass absorber, made of CFRP, whose fundamental characteristics are strongly variable through the application of piezoelectric transducers, connected to several electric circuits which consist of combinations of a resistance, inductance, and negative capacitance. This new design of a tunable vibration absorber shows very interesting characteristics, like no moving parts or active devices and an adaptable resonance frequency and damping level with very low energy consumption, which could have an important use in technical applications requiring vibration reduction. The design optimization, regarding the application of piezoelectric elements on the host structure, using the finite element method, aimed at the maximization of the generalized electromechanical coupling coefficient. The primarily predicted value of 0.34 could not be experimentally obtained, mainly because the elastic bonding between the clamp and the piezoelectric patches was not taken into account during the optimization. The achieved value of 0.26 still provides a good basis for the following evaluation of different shunting techniques. After having setup the prototype of the absorber with the numerically identified layout and geometry, the model was updated according to the experimental analysis.

In order to analyze the shunt parameters, a coupled analytical model has been derived from the updated finite element model, which is capable of efficiently predicting the effect of the electric circuit on the absorber

characteristics. The calculated results with an idealized negative capacitance were successfully validated by experimental analyses for the R-shunt, the RL-shunt, and the RLC-shunt.

The experimental shaker tests with the C-shunted absorber revealed that the assumption of an ideal negative capacitance is only valid, regarding the calculation of the shift of Eigenfrequency. This has also been experimentally validated with good precision. Regarding the levels of amplitude at the absorption frequency, an extended model for the NIC circuit has to be used, especially for higher tuning ratios. When including the electric components of the circuit, the overall behavior of the absorber is predicted quite well.

The damping characteristics of a mechanical absorber were modified by connecting an R-shunt to piezoelectric transducers. Furthermore, by applying an RL- and RLC-shunt the relative movement of the oscillating mass to the absorbers basement was reduced to a large extent. Finally, the absorber's Eigenfrequency was successfully shifted by applying a negative capacitance shunt. The lowest attainable Eigenfrequency was 24.3 % of the shunted absorber with open circuit electrodes.

Acknowledgments The research presented in this paper is funded by the German federal state of Hessen (project "LOEWE Zentrum AdRIA: Adaptronik—Research, Innovation, Application", Grant III L 4—518/14004(2008)) and the European Commission via the FP7 Marie Curie ITN (GRESIMO Project, GA 290050). This financial support is gratefully acknowledged.

Open Access This article is distributed under the terms of the Creative Commons Attribution 4.0 International License (http://creativecommons.org/licenses/by/4.0/), which permits unrestricted use, distribution, and reproduction in any medium, provided you give appropriate credit to the original author(s) and the source, provide a link to the Creative Commons license, and indicate if changes were made.

References

1. Frahm, H.: Device for damping vibrations of bodies. United States Patent 989958 (1911)
2. Ormondroyd, J., Den Hartog, J.: The theory of the vibration absorber. Trans. Am. Soc. Mech. Eng. (49), A9–A22 (1928)
3. Kela, L., Vähäoja, P.: Recent studies of adaptive tuned vibration absorbers/neutralizers. Appl. Mech. Rev. **62**(9), 060801–9 (2009)
4. Konstanzer, P., Jänker, P., Storm, S.: A piezo inertial force generator optimized for high force and low frequency. Smart Mater. Struct. **16**(4) (2007)
5. Sabirin, C.R., Röglin, T., Mayer, D.: Design and control of adaptive vibration absorbers mounted on an air conditioning compressor. In: Proceedings of the 8th International Conference on Structural Dynamics, EURODYN 2011, Leuven (2011)
6. Hagood, N.W., von Flotow, A.: Damping of structural vibrations with piezoelectric materials and passive electrical networks". J. Sound Vib. **146**(2), 243–268 (1991)
7. Davis, C.L., Lesieutre, G.A.: An actively tuned solid-state vibration absorber using capacitive shunting of piezoelectric stiffness. J. Sound Vib. **232**(3), 601–617 (2000)
8. Neubauer, M., Oleskiewicz, R., Popp, K., Krzyzynski, T.: Optimization of damping and absorbing performance of shunted piezo elements utilizing negative capacitance. J. Sound Vib. **298**(1–2), 84–107 (2006)
9. de Marneffe, B., Preumont, A.: Vibration damping with negative capacitance shunts: theory and experiment. Smart Mater. Struct. **17** (2008)
10. Forward, R.L.: Electronic damping of vibrations in optical structures. Appl. Opt. **18**(5), 690–697 (1979)
11. Tang, J., Wang, K.W.: Active-passive hybrid piezoelectric networks for vibration control: comparisons and improvement. Smart Mater. Struct. 794–806 (2001)
12. Antoniou, A.: Realisation of gyrators using operational amplifiers and their use in RC-active-network synthesis. Proc. IEE. **116**(11) (1969)
13. Forward, R.L.: Electromechanical transducer-coupled mechanical structure with negative capacitance compensation circuit. USA Patent US Patent Specification 4,158,787 (1979)
14. Date, M., Kutani, M., Sakai, S.: Electrically controlled elasticity utilizing piezoelectric coupling. J. Appl. Phys. **87**(2) (2000)
15. Behrens, S., Flemin, A.J., Moheimani, S.O.R.: A broadband controller for shunt piezoelectric damping of structural vibration. Smart Mater. Struct. **12**, 18–28 (2003)
16. Jones, B.K., Santana, J., McPherson, M.: Negative capacitance effects in semiconductor diodes. Solid State Commun. **107**(2), 47–50 (1998)
17. Manzoni, S., Moschini, S., Redaelli, M., Vanali, M.: Vibration attenuation by means of piezoelectric transducer shunted to synthetic negative capacitance. J. Sound and Vib. **331**(21), 4644–4657 (2012)